Neuron, Vol. 23, 105–114, May, 1999, Copyright ©1999 by Cell Press

lynx1, an Endogenous Toxin-like Modulator of Nicotinic Acetylcholine Receptors in the Mammalian CNS

Julie M. Miwa,* Ines Ibañez-Tallon,*
Gregg W. Crabtree,‡ Roberto Sánchez,†
Andrej Šali,† Lorna W. Role,‡
and Nathaniel Heintz*§
*Howard Hughes Medical Institute
Laboratory of Molecular Biology
†Laboratory of Molecular Biophysics
The Rockefeller University
New York, New York 10021
‡Department of Anatomy
Center for Neurobiology
Columbia University
New York, New York 10032

Summary

Elapid snake venom neurotoxins exert their effects through high-affinity interactions with specific neurotransmitter receptors. A novel murine gene, *lynx1*, is highly expressed in the brain and contains the cysteine-rich motif characteristic of this class of neurotoxins. Primary sequence and gene structure analyses reveal an evolutionary relationship between *lynx1* and the *Ly-6/neurotoxin* gene family. lynx1 is expressed in large projection neurons in the hippocampus, cortex, and cerebellum. In cerebellar neurons, lynx1 protein is localized to a specific subdomain including the soma and proximal dendrites. lynx1 binding to brain sections correlates with the distribution of nAChRs, and application of lynx1 to *Xenopus* oocytes expressing nAChRs results in an increase in acetylcholine-evoked macroscopic currents. These results identify lynx1 as a novel protein modulator for nAChRs in vitro, which could have important implications in the regulation of cholinergic function in vivo.

Introduction

The correct function of neuronal circuits involves the precise regulation of neurotransmitter receptor action. In addition to classical studies that have identified a variety of secreted peptides (Matthes et al., 1998) and hormones (Im et al., 1990) that influence receptor activity, exogenous toxins have been found that bind to and regulate the function of specific neurotransmitter receptors. For example, the snake venom neurotoxins exert their action through high-affinity binding to nicotinic (Chen and Patrick, 1997) and muscarinic (Jolkkonen et al., 1994) acetylcholine receptors (AChRs). The physiological relevance of toxin action rests on the idea that these molecules have evolved from endogenous genes operating in normal cellular pathways (Ohno et al., 1998). Functional homologs to important mammalian signaling molecules, including nerve growth factor (NGF) (Inoue et al., 1991), acetylcholinesterases (Cousin et al., 1998), and phospholipases (John et al., 1994), have been identified as components of snake venom. In some cases, evidence for a direct evolutionary relationship between a mammalian gene and a specific toxin gene family has been obtained. For example, a functional relationship between hemolytic snake venom toxins and cellular phospholipases has been recognized from the earliest studies of these molecules (Strydom, 1979) and has been strongly supported by more recent protein sequence comparisons and evidence of gene duplication of this large gene family (Davidson and Dennis, 1990; Kini and Chan, 1999). An evolutionary and functional relationship between snake venom sarafotoxins and vertebrate endothelins has also been proposed (Kochva et al., 1993). These examples suggest the existence of endogenous counterparts in cases where functional homologs for toxin genes have not been identified.

One class that lacks functional homologs is the elapid snake venom neurotoxins that bind to muscle and brain AChRs. Examples include α-bungarotoxin (αBtx), which binds to and inhibits nAChRs (Chen and Patrick, 1997), and the muscarinic AChR toxin MT3 (Jolkkonen et al., 1994). An evolutionary relationship has been proposed between this class of neurotoxin and the mammalian *Ly-6* genes based on sequence similarity (Fleming et al., 1993), conservation of a signature motif, similar tertiary conformation, and common gene structure (Gumley et al., 1995a). The *Ly-6* genes code for cell surface accessory proteins expressed mainly on cells of the immune system. They are thought to participate in diverse recognition and adhesive functions, such as T cell activation, lymphocyte homing, and leukocyte migration (Gumley et al., 1995a; Hanninen et al., 1997). Despite the evolutionary and structural similarities, no functional similarity between the elapid snake toxins and the *Ly-6* genes has been established (Gumley et al., 1995a), due in part to their disparate sites of action.

In this study, we report the discovery of a novel murine gene, *lynx1*, similar to the snake venom neurotoxins and the Ly-6 antigens of the immune system. A direct evolutionary relationship between *lynx1* and the *Ly-6/neurotoxin* superfamily of genes (Chang et al., 1997a and 1997b) is supported by primary sequence and gene structure analyses. *lynx1* is highly expressed in several discrete neuronal populations in the brain, and the distribution of lynx1 binding sites is similar to that of nAChRs. To test whether lynx1 might be functionally homologous to the venom toxins, we analyzed its effects on nAChR responses in *Xenopus* oocytes. We report that lynx1 can act as a novel modulator of nicotinic receptors in vitro, raising the interesting possibility that lynx1 participates in a novel mechanism for cholinergic regulation in vivo.

Results

lynx1 Encodes a Novel Member of the *Ly-6/αBtx* Gene Family

In the course of a screen for CNS-specific, developmentally regulated cDNAs, we identified a novel cDNA,

§To whom correspondence should be addressed (e-mail: heintz@rockvax.rockefeller.edu).

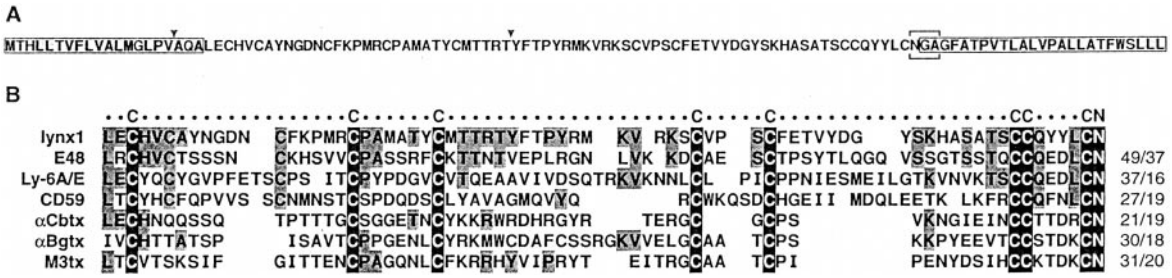

Figure 1. The *lynx1* ORF Encodes a GPI-Linked Cell Surface Molecule with Homologies to the *Ly-6/αBtx* Superfamily

(A) Predicted amino acid sequence of the *lynx1* ORF is shown. The boxed N terminus demarcates the putative signal sequence. The C-terminal transmembrane domain that is cleaved during the processing of the GPI anchor is boxed. The consensus recognition sequence for the attachment of the GPI moiety is indicated in brackets (Udenfriend and Kodukula, 1995). Nonpolar residues are shaded. Arrowheads designate the position of the intron breaks in the *lynx* gene.

(B) Amino acid sequence homology between lynx1 and members of the *Ly-6/αBtx* gene superfamily. Family members comprise two groups: the lymphocyte cell surface antigens E48, Ly-6 A/E, and CD59, and the elapid snake venom toxin peptides α-cobratoxin (αCtx), αBtx, and m3 toxin (M3tx). The putative mature amino acid sequence only was used for these alignments. The Ly-6 consensus motif is shown above. Residues corresponding to this consensus are shaded in black. Residues matching the lynx1 polypeptide are shaded in gray. Numbers at the right indicate the percentage similarity and identity, respectively, to the lynx1 mature polypeptide.

GC26, expressed in the mouse cerebellum (Kuhar et al., 1993). To further pursue the characterization of *GC26*, we undertook the isolation of a full-length *GC26* cDNA clone (4.1 kb) through several rounds of cerebellar cDNA library screening. Sequence analysis of this cDNA revealed a short (351 bp) open reading frame (ORF) encoding a protein of a predicted size of 11 kDa (Figure 1). This ORF was verified by in vitro translation of the mRNA encoded by *GC26* and electrophoretic analysis of the resulting protein product (data not shown). Analysis of the predicted polypeptide sequence demonstrated that *GC26* codes for a protein containing an N-terminal signal sequence and a hydrophobic C-terminal domain matching the consensus for addition of a GPI anchor (Udenfriend and Kodukula, 1995; Figure 2A). The N terminus encoded a consensus signal sequence that was later demonstrated to be functional by transfection of a fusion construct containing the signal sequence and the mature polypeptide in frame with the hemagglutinin epitope (HA). In these cells, mature HA-tagged product was secreted into the culture supernatant (data not shown).

Database searches of the GC26 amino acid sequence (Altschul et al., 1990) demonstrated similarity (18%–50%) to a family of small cysteine-rich proteins comprising the secreted elapid snake venom neurotoxins (Hung et al., 1998) and the Ly-6 GPI-linked cell surface accessory molecules of the immune system (Figure 2B; Fleming et al., 1993; Brakenhoff et al., 1995; Gumley et al., 1995a, 1995b). A characteristic feature of the Ly-6 and the α-neurotoxin proteins is the presence of a cysteine-rich consensus motif consisting of an N-terminal leucine/isoleucine, eight cysteines, and a C-terminal asparagine. Alignment of GC26 with the Ly-6 proteins and the snake neurotoxins demonstrated that GC26 contains this signature motif (Figure 2B). The overall sequence similarity between *lynx1* and the *Ly-6/neurotoxin* gene family, and the conservation of this signature cysteine-rich motif, prompted us to name the GC26 polypeptide lynx1 (*Ly*-6/*n*eurotox*in*).

Structural data for members of this superfamily, such as CD59, αBtx, and cobratoxin, demonstrate a strikingly similar tertiary structure (Le Goas et al., 1992; Basus et

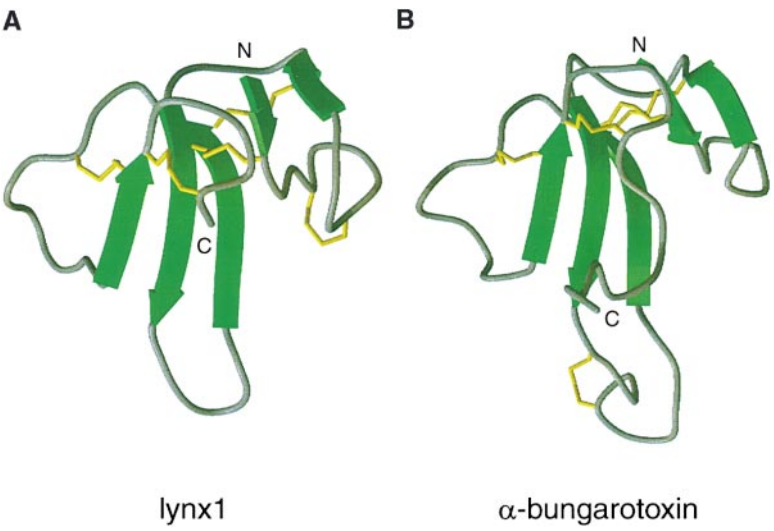

Figure 2. Comparison of the lynx1 Model and the αBtx Experimental Structure

(A) Three-dimensional model of lynx1. Strands are shown as green arrows and disulfide bridges are colored yellow.

(B) Experimental NMR structure of αBtx (PDB code 1abt). The orientation and coloring is the same as for lynx1. N- and C-terminal ends of the molecules are labeled.

al., 1993; Fletcher et al., 1994), despite their low overall sequence similarity. This is due to the fact that the conserved cysteine residues that constitute the Ly-6/neurotoxin motif are critical determinants in the overall topology of these molecules. The disulfide bonds created by these conserved cysteines create a rigid β sheet core, out of which three variable loops emerge. Conservation within lynx1 of these critical residues suggest that lynx1 is structurally related to the snake toxins and can adopt its receptor binding fold. To test whether or not lynx1 adopts the snake toxin fold, comparative models of lynx1 were built using three different template structures with the snake toxin fold (Figure 2). Experimental structures of CD59, αBtx, and cardiotoxin were used independently and in combination with each other to produce four different models. The evaluation of the models indicated that all four of them are reliable with a probability of having the correct fold of 0.84, 0.91, 0.93, and 0.94 for the best models based on CD59, cardiotoxin, αBtx, and all three templates, respectively. This indicates that the best individual template structure for lynx1 is αBtx, although the model based on all three templates is the best model produced. This is not surprising, since the use of more than one related template usually improves the quality of the resulting comparative model (Sánchez and Šali, 1997). The false-positive rate of the evaluation procedure for models of this size (70 residues) is only 7% (Sánchez and Šali, 1998). As a negative control, a model for lynx1 was built based on bovine pancreatic trypsin inhibitor (BPTI), a small disulfide-rich protein that does not adopt the snake toxin fold. The probability of having the correct fold for this model was <0.5 (i.e., 0.28), supporting the prediction that lynx1 can in fact adopt the snake toxin fold.

An evolutionary relationship between the *Ly-6* genes and the snake venom toxins has been proposed based on conservation of intron–exon boundaries in the coding portions of these genes (Fuse et al., 1990; Chang et al., 1997a and 1997b). The *Ly-6* and α-*neurotoxin* genes have a conserved intron dividing the signal sequence into two exons, and another intron interrupting the mature polypeptide between the third and fourth conserved cysteine residues. To assess whether *lynx1* belongs to the *Ly-6/neurotoxin* superfamily, we determined the *lynx1* gene structure. *lynx1* genomic clones were obtained through screening a bacterial artificial chromosome library (BAC) of mouse genomic DNA. A *lynx1*-containing BAC was verified by Southern analysis, subcloned and sequenced, and compared against the *lynx1* cDNA sequence. As shown, the intron–exon boundaries in the *lynx1* gene are located within the putative signal sequence and in the region corresponding to the second loop in *lynx1*, as previously documented for *Ly-6* and *cobratoxin* genes (Figures 3A and 3B). In addition, several of the mammalian *Ly-6* genes have been independently cloned, and genetic mapping experiments show that many of these family members map to the same chromosomal position in the mouse genome (Gumley et al., 1995a). Genetic mapping of *lynx1* in mice determined that it maps to the *Ly-6* gene cluster (J. M. M., C. F. Fletcher, N. A. Jenkins, N. G. Copeland, and N. H., submitted). We conclude that *lynx1* is evolutionarily related to both the *Ly-6* gene and the elapid snake neurotoxin gene and that it is a novel member of this superfamily.

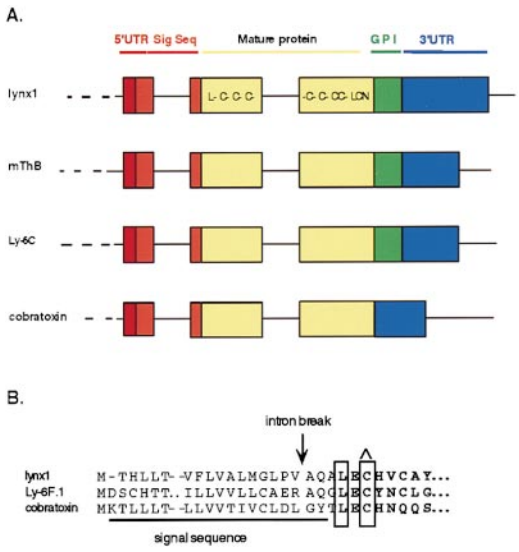

Figure 3. The *lynx1* Gene Shows Similar Gene Organization with the *Ly-6/Neurotoxin* Gene Superfamily

(A) Representation of the coding exons of the *lynx1* gene as compared to members of the *Ly-6* superfamily, *mThB* (Gumley et al., 1995b), *Ly-6C* (Fleming et al., 1993), and *cobratoxin* (Chang et al., 1997b). These intron breaks occur in similar positions as those of the *Ly-6* genes *mThB* (Gumley et al., 1995b), *E48* (Brakenhoff et al., 1997), and *erabutoxin* (Fuse et al., 1990). In (A), the exons are represented as boxes and are not to scale. The red shading within the boxes represents the 5′ UTR, the orange shading represents the signal sequence (Sig Seq), the yellow shading represent the mature protein, the green shading represents the hydrophobic GPI consensus sequence, and the blue shading represents the 3′ UTR. The conserved residues that make up the consensus motif are designated within the yellow portion of the second and third exons.

(B) One highly conserved intron break occurs within the signal sequence, three residues prior to the first leucine of the mature polypeptide. The signal sequence is underlined, and the sequence corresponding to the mature protein is designated in bold. The residues of the consensus are boxed, and the starting residue of the mature protein, leucine, is designated with a hatch. The arrow indicates the position of the intron break in the genomic sequence.

lynx1 Is Highly Expressed in the Mammalian CNS

To gain insight into the potential role of lynx1 in vivo, we first determined its pattern of expression. Northern blot analyses demonstrated that *lynx1* mRNA is highly enriched in the brain, although low levels can be detected in other tissues such as kidney (Figure 4A), heart, and thymus (data not shown). Northern blot analyses at various stages of cerebellar development demonstrate that *lynx1* is expressed at very low levels at birth and undergoes a marked upregulation between postnatal days 10 and 20 (Kuhar et al., 1993). In situ hybridization to adult brain sections revealed that *lynx1* is highly expressed in subsets of neurons in multiple brain structures (Figure 4B), including Purkinje cells and deep nuclear neurons of the cerebellum (Figures 4Ba and 4Bb), deep layer pyramidal neurons in the cerebral cortex (Figure 4Bd), CA3 pyramidal cells and hilar neurons of the

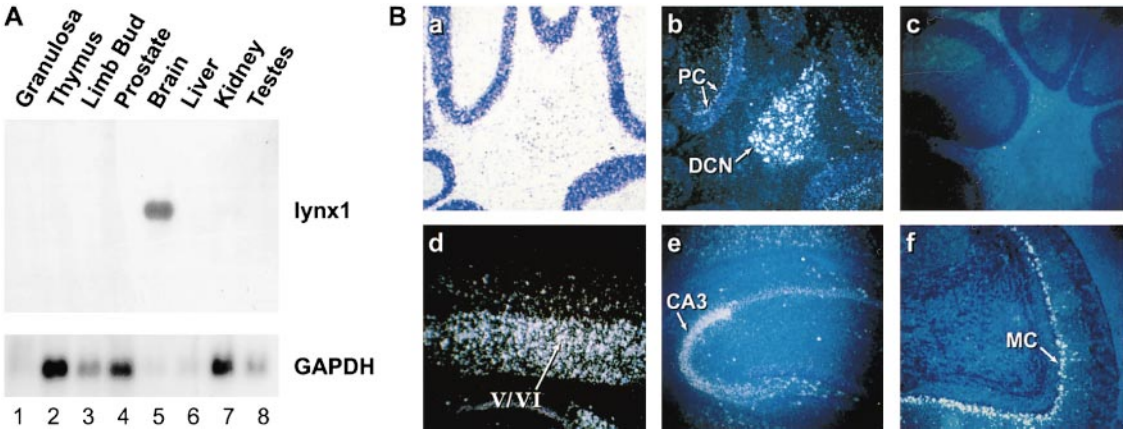

Figure 4. Expression of the *lynx1* Gene Is Highly Enriched in Specific Regions

To test the expression pattern of the *lynx1* message, multiple tissues were tested by Northern analysis, and in situ hybridization was carried out on mouse brain sections.

(A) Northern blot analysis of *lynx1* gene expression. Poly(A)$^+$ RNA from adult murine tissues (as indicated) was probed with the *lynx1* cDNA (upper panel) and with a GAPDH loading control (lower panel). *lynx1* is highly expressed in the brain, with lower levels of expression in the kidney. The *lynx1* cDNA hybridizes to a band of ~4.0 kb.

(B) In situ hybridization analysis demonstrates *lynx1* expression in subsets of neurons across multiple circuits in the brain.

(a–b) Bright- and dark-field photomicrographs, respectively, of the same field of the mouse cerebellum reacted with the *lynx1* antisense ^{35}S-labeled riboprobe.

(b) *lynx1* is detected in the Purkinje cell body layer (PC) and the deep cerebellar nuclei (DCN).

(c) No signal is observed with the sense control probe.

(d–f) *lynx1* expression is high in the deep layers of the cerebral cortex (V/VI) (d), CA3 pyramidal neurons of the hippocampal formation (e), and mitral cells of the olfactory bulb (MC) (f).

hippocampus (Figure 4Be), and mitral cells of the olfactory bulb (Figure 4Bf). No detectable signal was observed with the sense control probe (Figure 4Bc). High-resolution colorimetric in situ hybridization analysis demonstrated expression within individual neurons (Figures 5A–5D) in these structures and revealed dramatic differences in the levels of expression of *lynx1* between specific neuronal populations.

lynx1 Is Expressed in a Neuronal Subdomain

We next examined lynx1 protein distribution by immunocytochemistry to determine if lynx1 is localized to a specific subdomain within individual neurons. Cerebellar Purkinje cells are a useful model system for this analysis, as they are highly polarized neurons with an elaborate dendritic tree that is compartmentalized into discrete subdomains defined by segregated afferent types. These subdomains include proximal dendrites receiving inputs from climbing fibers, diffuse cholinergic terminals, and inhibitory stellate and basket neurons in addition to the distal dendritic compartment, innervated by parallel fibers onto dendritic spines (Larramendi and Viktor, 1967). Immunostaining with the lynx1 antiserum revealed that lynx1 is present on Purkinje cell soma and proximal dendrites (Figures 6A and 6C), in contrast to the

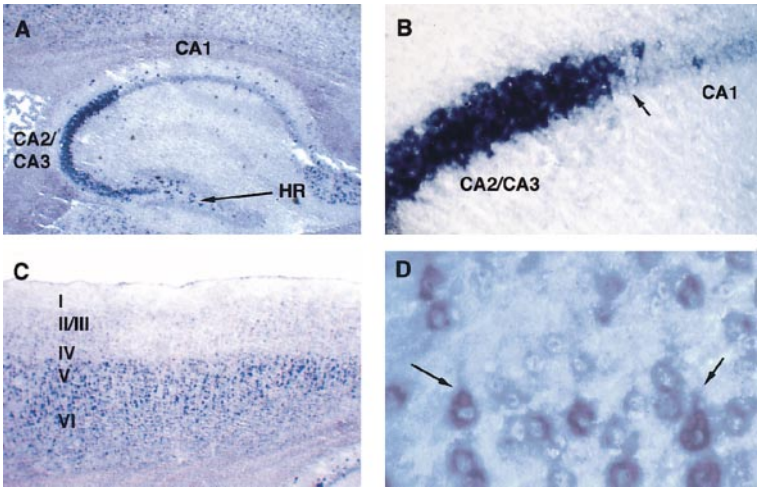

Figure 5. High Levels of Expression of *lynx1* in Discrete Neuronal Subpopulations; Colorimetric In Situ Hybridization Detects *lynx1* mRNA in Individual Neurons

(A–B) Message levels in the hippocampal formation are very high in neurons of the CA2/CA3 region of the hippocampus, at medium and high power, respectively. High levels of message are found within individual neurons of the hilar region (HR).

(C) Message levels show laminar differences in the cerebral cortex, with highest levels of expression found in the lower layers (V/VI), no detectable message in layer IV, and little to no detectable message in the upper layers (I/II/III).

(D) High levels of message are detected in individual neurons of the cortex. Substrate deposition in the cytoplasm reveals pyramidal neurons that are highly positive for *lynx1* message (arrows).

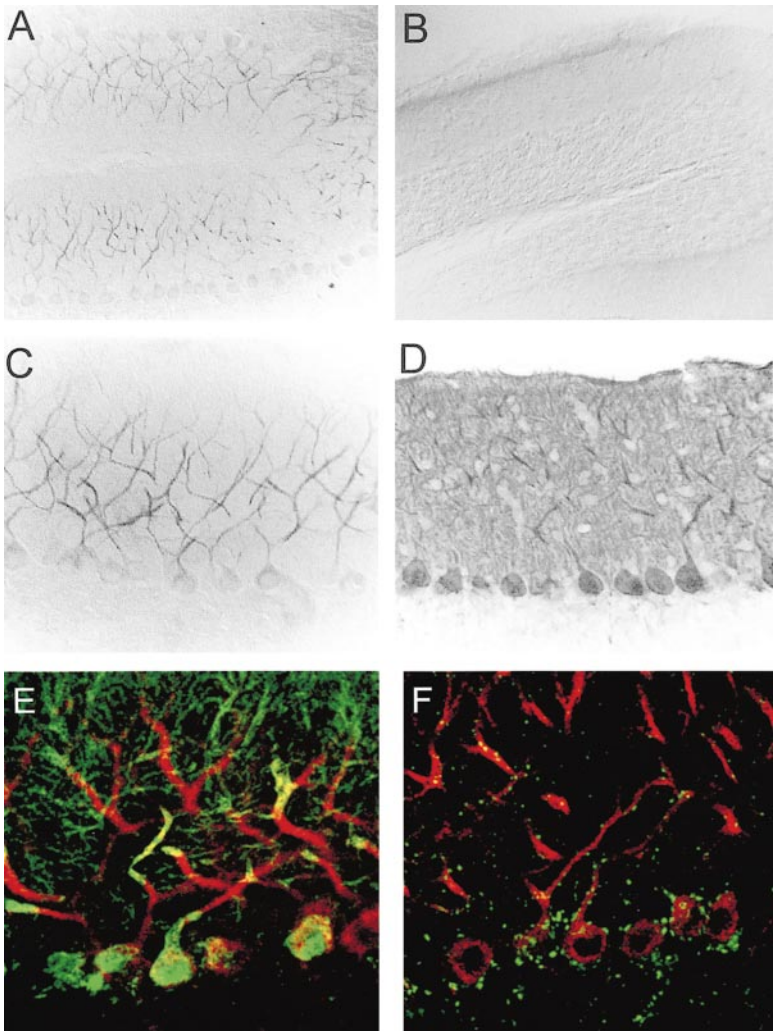

Figure 6. The lynx1 Protein Is Localized to a Subdomain within the Dendritic Arbor of Purkinje Cells of the Cerebellar Cortex

(A–D) Immunocytochemistry on mouse cerebellar sections shows specific localization of the lynx1 protein.

(A and C) Low- and higher-power photomicrographs of mouse cerebellum immunostained with lynx1 peptide antiserum. lynx1 expression is confined to proximal dendrites and soma of Purkinje cells in the cerebellar cortex.

(B) No staining is observed with preimmune control serum.

(C and D) Adjacent serial sections reacted with anti-lynx1 and anti-calbindin antisera, respectively, showing the limited distribution of lynx1 as compared to calbindin.

(E and F) Immunofluorescence analysis of lynx1 protein localization.

(E) Calbindin antiserum (green) labels the complete dendritic arbor of Purkinje cells, including the finely articulated spiny branchlets, whereas lynx1 antiserum (red) labels only the proximal dendritic branches of these neurons.

(F) The profile of inhibitory synapses onto Purkinje cells, as revealed by anti-GAD immunoreactivity (green), shows inhibitory synaptic termini closely apposed to lynx1-positive postsynaptic domains (red). This is in contrast to the profile of all synapses, which is densely packed and evenly distributed across the molecular layer of the cerebellum and not confined to a dendritic subfield (data not shown).

staining observed with antiserum against the calcium binding protein calbindin, which labels the entire Purkinje cell dendritic arbor (Figure 6D), and with preimmune controls, which show no signal (Figure 6B). This distribution is also observed by double immunofluorescence staining and visualization with the confocal microscope comparing the distribution of lynx1 and calbindin in single Purkinje cells (Figure 6E). These data indicate that lynx1 is localized to the proximal somatodendritic compartment, which receives most of the inhibitory inputs onto Purkinje cells.

We also compared the distribution of lynx1 protein within this domain to glutamic acid decarboxylase (GAD), which is highly expressed in presynaptic terminals of inhibitory interneurons. Comparison of GAD distribution with the localization of lynx1 demonstrates lynx1-positive sites in apposition to inhibitory presynaptic terminals, confirming that lynx1 is present in the proximal postsynaptic compartment (Figure 6F). lynx1, however, displays a much broader distribution than the synaptic regions revealed by GAD staining. Thus, lynx1 protein is maximally expressed in a neuronal subdomain that correlates with the distribution of a defined subset of afferent inputs, but it is not restricted to discrete postsynaptic sites within this subdomain.

lynx1 Binds to Specific CNS Neurons

To assess whether lynx1 functions through interactions with a specific binding partner, a receptor affinity probe was generated by cloning lynx1 in frame with the Fc portion of human immunoglobulin (lynx1/Fc). The lynx1/Fc fusion protein was used to perform binding assays on sections of adult cerebellar tissue. Binding of lynx1 was detected on the Purkinje cell soma and proximal dendrites, as well as on basket and stellate neurons resident in the molecular layer of the cerebellar cortex (Figures 7A and 7B). This binding was specific, since purified lynx1 competed the binding of the lynx1/Fc fusion, and no binding was observed using the Fc fragment alone (Figures 7C and 7D). The pattern of lynx1 binding includes the lynx1-positive subdomain of cerebellar Purkinje cells, as well as interneuron cell bodies that do not express significant levels of lynx1. Interestingly, this pattern of binding is similar to the distribution of nAChRs reported in the literature and as assayed by α7 nAChR immunoreactivity (data not shown; Dominguez Del Toro et al., 1994). These results strongly suggest that lynx1 can form heterotypic interactions with a CNS receptor, but they do not rule out homotypic interactions between lynx1 molecules on the surface of lynx1-expressing cells.

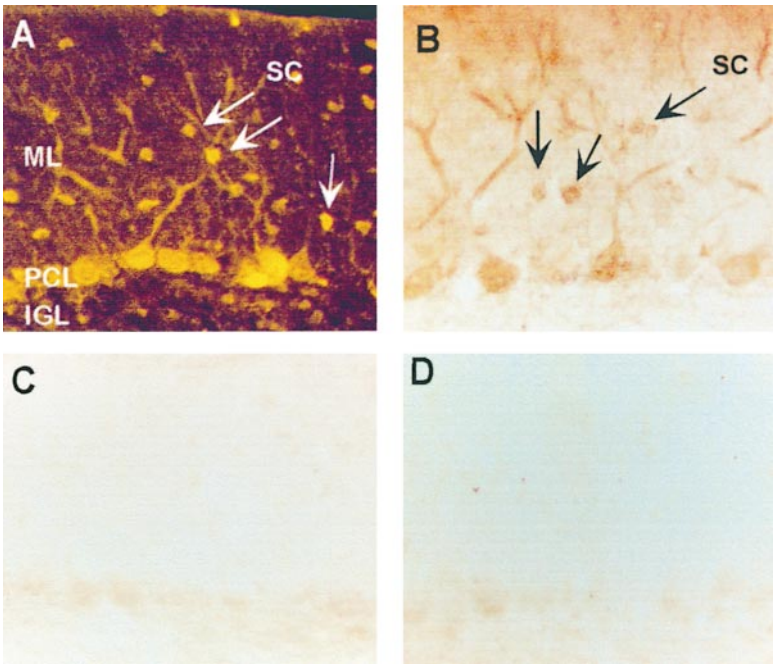

Figure 7. Localization of lynx1 Binding Sites in the Cerebellar Cortex

(A and B) Binding of lynx1/Fc fusion protein to sections of the cerebellar cortex detected either by indirect immunofluorescence (A) or immunocytochemistry (B). In both cases, Purkinje cell somata and proximal dendrites, as well as basket and stellate cell bodies (arrows), are detected.

(C) Binding of the Fc fragment to cerebellar slices reveals no specific labeling.

(D) Preincubation of sections with recombinant *lynx1* specifically inhibits the binding of the lynx1/Fc fusion protein.

lynx1 Can Modulate Nicotinic Acetylcholine Receptor Function In Vitro

To test whether lynx1 functions through AChRs, we examined ACh-elicited macroscopic current responses in control and lynx1-treated *Xenopus* oocytes expressing recombinant $\alpha4\beta2$ nAChR subunit cRNAs (Figure 8). Injected oocytes were assayed in voltage clamp, and inward current responses to ACh were measured for ~30 min before and after treatment with purified lynx1. Sequential preapplication responses to ACh (1 mM, 20 s) differed by less than 2%–3% when trials were separated by 5 min intervals. After a stable baseline was established, a 20 s pulse of lynx1 solution was applied, after which the first test pulse of ACh was delivered. Application of lynx1 enhanced the amplitude of the ACh-evoked macroscopic currents by 30%–40% compared with nontreatment or column-passed PBS controls ($n = 8$ oocytes, mean increase ~35%, $p = 0.001$). lynx1 application augmented ACh-evoked currents within the first or second posttreatment trials and exhibited similar activity with all ACh concentrations tested (10 μM to 1 mM). Similar results were obtained on $\alpha7$ homomers, and with multiple lynx1 preparations obtained from different heterologous expression systems, including conditioned media from mammalian cells transfected with lynx1–HA or lynx1–alkaline phosphatase (AP) fusion constructs, and bacterially expressed lynx1 (data not shown). During the 20 s preapplication of lynx1, in the absence of ACh,

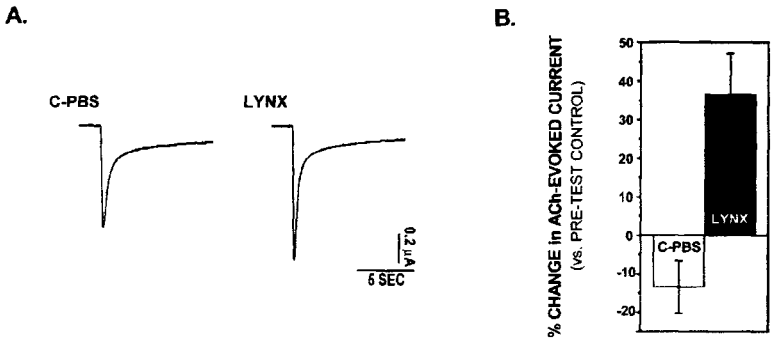

Figure 8. lynx1 Increases ACh-Gated Macroscopic Current Responses

ACh-elicited macroscopic current responses in voltage-clamped *Xenopus* oocytes expressing $\alpha4\beta2$ nAChRs.

(A) Representative macroscopic current responses to 1 mM ACh under control conditions (above) and in the second ACh trial, following lynx1 treatment.

(B) Plot of cumulative results from eight experiments. Column-purified lynx1 (1%, in oocyte recording media; see Experimental Procedures) significantly increases the amplitude of macroscopic current responses to ACh (1 mM, 20 s application, 5 min intertrial interval). Each experiment represents 20–60 ACh-evoked responses per condition including the pretreatment controls (set to 100%) column-purified lynx1 and a PBS control (cPBS). The latter control solution is the running buffer for the lynx1 purification column, collected following isolation of the active lynx1 fractions.

no lynx1-evoked currents were detected in five of the six lynx1 preparations tested. As lynx1 does not reproducibly elicit currents when applied alone, we conclude that lynx1 is not a ligand or neurotransmitter but that it has the capacity to modulate receptor function in the presence of its natural ligand, ACh. Taken together, these data demonstrate that lynx1 can act as a modulator of AChR function in vitro. Furthermore, the action of lynx1 on these receptors is distinct from that of the neurotoxins, since in the presence of lynx1 we observe an increase rather than a decrease in ACh-evoked macroscopic currents through these receptors.

Discussion

The data we have presented in this study identify *lynx1* as a novel member of the *Ly-6/neurotoxin* gene superfamily, highly expressed in discrete neurons of the CNS. In vitro tests reveal that application of lynx1 to nAChRs results in an increase in ACh-evoked currents through these receptors. These results demonstrate that lynx1 can act as a novel modulator of AChR function, which could have important implications for cholinergic function in vivo.

The assignment of *lynx1* to the *Ly-6/neurotoxin* gene superfamily is based on overall sequence similarity, conservation of the cysteine-rich consensus motif, and common gene structure with members of this superfamily. Given the importance of the conserved cysteines as critical determinants of topology, their presence in lynx1 suggested it might adopt a similar three-looped "toxin fold." This led us to explore the possibility that lynx1 may bind to specific receptors in the CNS. Interestingly, binding of lynx1 to brain sections revealed a pattern similar to that of the nAChRs. For example, in the cerebellum, lynx1 binds to Purkinje cell proximal compartments and to interneurons presynaptic to Purkinje cells, matching the localization of α7 AChRs (Dominguez Del Toro et al., 1994). As lynx1 is detected in Purkinje cells alone, these data demonstrate that lynx1 can interact with a binding protein present in cell types that do not express significant levels of lynx1. Thus, this establishes that lynx1 can form heterotypic interactions and that nAChRs are a probable candidate for this interaction. This, taken together with our supposition that lynx1 was the functional homolog to snake toxins, prompted us to test the effect of lynx1 on nAChRs in vitro. This assay reveals that lynx1 can enhance the function of these receptors in the presence of its natural ligand, identifying lynx1 as a novel modulator of nAChRs in vitro. Neuropeptide modulators of receptor function, such as somatostatin and opioids, are released from the presynaptic terminals into the synaptic cleft (Maley et al., 1987; Garside and Mazurek, 1997), whereas lynx1 is normally present at the cell surface as a GPI-anchored protein. This raises the possibility, therefore, that lynx1 is operating on nAChRs via a novel mechanism.

The observation that both nAChRs and lynx1 are expressed at extrasynaptic sites on the soma and proximal dendrites of Purkinje cells may be an important clue to the in vivo function of lynx1. One of the main characteristics of the cholinergic projections from the brainstem are their wide and diffuse distribution throughout the nervous system. The mode of action of ACh in the CNS is unusual in that the majority of both cholinergic terminals from central projections and AChRs on target cells are diffusely distributed and extrasynaptic (Contant et al., 1996), although direct action of ACh at central synapses has been demonstrated (McGehee et al., 1995; Gray et al., 1996). This has led to the hypothesis that cholinergic terminals modulate cell excitability through release of ambient levels of ACh (Descarries et al., 1997). One intriguing possibility is that lynx1 is important for regulating the response of extrasynaptic receptors to these ambient levels of ACh in selected populations of neurons. Since cholinergic inputs have been implicated in many important functions, including learning and memory, attention, and sleep–wake cycles (Picciotto et al., 1995; Everitt and Robbins, 1997; Robbins, 1997; Changeux et al., 1998; Coull, 1998), and since the loss of central cholinergic function may be an important factor in the decline of cognitive function with age (Gallagher and Rapp, 1997) and in Alzheimer's disease (Robbins et al., 1997; Geula, 1998), an involvement of lynx1 in modulation of cholinergic function in vivo would be very important.

Further investigations will be required to understand the mechanism of action of lynx1 on AChRs in vitro, including its possible direct binding to AChR subunits, its specificity for AChR subtypes, and the detailed mechanism whereby it modulates AChR function. Moreover, while our data point to AChR as a likely target for lynx1 actions, we cannot rule out the possibility that other receptors or binding proteins could be the physiological targets for lynx1. Genetic manipulations and behavioral tests will ultimately be required to elucidate the precise function of lynx1 in vivo. Finally, the discovery of lynx1 as a novel toxin-like CNS protein and the demonstration of its impact on nicotinic AChR function raise the issue of the existence of other "prototoxin" genes and their possible roles in CNS function. Given the large number of protein toxins identified in snakes and invertebrates and their wide-ranging specificity for different receptors, channels, and proteins (Dufton and Harvey, 1989; Adem and Karlsson, 1997; Harvey, 1997; Kumar et al., 1997), it seems probable that other genes of this type may be present in mammals. Studies of these putative prototoxin genes may reveal new molecular mechanisms that have a critical impact upon vertebrate brain function.

Experimental Procedures

cDNA Library Screening

Library screening was conducted on an oligo-dT primed λ zap cDNA library synthesized from adult murine cerebellar RNA, using a 1.5 kb Sfi1-Not1 fragment from the *GC26* cDNA (*GC26-1*). The predicted amino acid sequence from the ORF of the full-length cDNA (*lynx1-3*) was used to search GenBank with tblastn and blastp search algorithms, using PAM250 and default parameters. Amino acid sequence alignments were performed using the ClustalW algorithm (MacVector, DNAstar).

Structural Modeling

Three-dimensional models of lynx1 were built automatically by the computer program MODELLER-5 (Šali and Blundell, 1993). MODELLER-5 implements comparative modeling by satisfaction of spatial restraints (Šali and Blundell, 1993). The input to MODELLER-5 was a multiple alignment of lynx1 with members of the snake toxin

fold family of known three-dimensional structure. The alignment was prepared by hand following the pattern of conserved cysteine residues. First, MODELLER-5 derived many distance and dihedral angle restraints on the lynx1 sequence from the alignment with the template proteins. One additional restraint was added manually to force a disulfide bridge between cysteine 6 and cysteine 11 in lynx1. Next, these homology-derived spatial restraints and CHARMM-22 energy terms (Brooks et al., 1983) enforcing proper stereochemistry were combined into an objective function. Finally, the variable target function procedure, which employs methods of conjugate gradients and molecular dynamics with simulated annealing, was used to obtain the three-dimensional models by optimizing the objective function. In each case, ten slightly different three-dimensional models were calculated by varying the initial structure.

Since the sequence similarity between lynx1 and the members of the snake toxin fold family is not striking, different members of that family were used as templates. Specifically, CD59 (PDB code 1erg), αBtx (1abt), and cardiotoxin (1tgx) were used individually and in combination with each other as structural templates. BPTI (6pti), another small disulfide-rich protein that does not adopt the snake toxin fold, was used as a template to test the ability of the evaluation procedure to detect incorrect folds. The reliability of the resulting models was predicted by a procedure based on statistical potentials of mean force (Sippl, 1993) and using the resulting scores to predict the probability that the models have the correct fold by a procedure described by Sánchez and Šali (1998).

Genomic Analysis

A 1.5 kb fragment of the 3′ UTR region (*GC26-1*) was used as a probe to screen a BAC library of mouse genomic DNA (Research Genetics) under stringent conditions (65°C, 0.2× SSC, 0.1% SDS). A *lynx1* gene–containing BAC clone (*BAClynx1-9*) was verified by Southern analysis using the *GC26-1* and the ORF of *lynx1-3* as probes. The BAC was PCR amplified using cDNA-specific primers, subcloned, and sequenced. Genomic sequence was compared against cDNA sequence to verify intron–exon boundaries.

Northern Blot

Tissue was dissected and frozen in liquid nitrogen; RNA was extracted in guanidinium–thiocyanate according to standard methods. Poly(A)$^+$ RNA was purified using oligo-dT chromatography. RNA (5 μg) was electrophoretically separated, blotted onto Genescreen nylon membrane, probed overnight at 42°C, and washed at a stringency of 0.5× SSC, 0.1% SDS at 65°C. The probe was made by random primed labeling of the *lynx1-3* ORF.

In Situ Hybridization

In situ hybridization analyses were conducted on 10 μm fresh frozen sections of adult mouse brain. *GC26-1*, the *lynx1* 3′ UTR, was used for these experiments. In the radioactive method, one million counts of ^{35}S-labeled riboprobe were applied to each section and washed to a stringency of 0.1× SSPE at 65°C. The slides were exposed and developed under standard conditions and counterstained with cresyl violet. In the colorimetric method, digoxigenin- (Dig-) labeled riboprobe was transcribed using 0.5 μm Dig–UTP (Boehringer-Mannheim) in the transcription reaction. Sections were incubated at 65°C overnight in hybridization buffer (50% formamide, 300 mM NaCl, 50 mM Tris, 1 mM EDTA, 1% Denhardt's reagent, 10% dextran sulfate, and 0.1 mg/ml yeast tRNA [pH 8.0]) and washed to a final stringency of 0.2× SSC at 65°C. Riboprobe was detected with anti-Dig Fab fragments conjugated to AP and NBT/BCIP/levamisole substrate mixture.

Immunocytochemistry

Peptide antibodies were generated from the peptide sequence TTRTYFTPYRMKVRKS. Antisera were screened by Western blots of bacterially expressed lynx1 fusion protein and on mouse cerebellar extracts. Briefly, a portion of the *lynx1* cDNA, corresponding only to the mature polypeptide, was cloned in frame to six histidines using the pet14b bacterial expression vector (Pet264). Transformed cells were induced, and protein was purified using Ni resin (Qiagen) and eluted. Adult mouse brains were perfused with 4% paraformaldehyde/PBS, sunk in 30% sucrose/PBS, and sectioned at 20 μm on a freezing microtome. The sections were blocked with 10% NGS, 0.05% Triton X-100 in PBS and incubated in anti-lynx1 antiserum for 1 hr at room temperature at a dilution of 1:8,000 or anti-calbindin antibodies (SWant) at 1:10,000. Antibody binding was visualized using the ABC Elite kit (Vector) according to the manufacturer's instructions and reacted with H_2O_2/DAB substrate.

Immunofluorescence

Sections were prepared as above. The lynx1 antiserum was used at 1:2,000 and detected with goat anti-rabbit secondary antibody conjugated to Cy3 (Jackson Immunochemicals). Double labeling with anti-GAD was performed at 1:1,000 (Boerhinger Mannheim) and detected with goat anti-mouse Cy5 at 1:800 (Jackson Immunochemicals). Labeling was imaged on a scanning laser confocal microscope (Zeiss).

Affinity Binding Assay

The *lynx1* cDNA corresponding to the mature lynx1 protein with its native signal sequence was cloned in frame 5′ to the Fc portion of human IgG (lynx1/Fc). The control used was a secreted, unfused Fc construct. Constructs were transfected and treated as above, then concentrated 1:20 in an Ultrafree-Biomax spin column (Millipore). The lynx1 fusion protein was normalized against the control by Western analysis. Binding experiments were performed on 50 μm vibratome sections of perfused mouse brains (as above). The sections were blocked in 10% NGS in PBS, reacted with lynx1/Fc for 1 hr, and washed. lynx1/Fc binding was detected with goat anti-human IgG Cy3 at 1:1,000 (Jackson Immunochemicals) and detected by epifluorescence microscopy using a rhodamine filter. Pet264 bacterial fusion protein was used for the competition experiments (see above).

lynx1 Preparation for Oocyte Recording

The *lynx1* cDNA corresponding to the lynx1 mature protein with its native signal sequence and without the GPI consensus sequence was cloned in frame with the HA epitope, downstream of the CMV promoter (referred to as CMV2611). CMV2611 constructs were transfected into 293T cells, which were cultured for 3 days before supernatants were harvested. HEPES (5 nM [pH 7.2]) was added to the cultured supernatants, which were then precipitated with 50% ammonium sulfate. The pellet was resuspended in PBS and fractionated on a Pharmacia Hiload Superdex 16/60 gel filtration column. lynx1-containing fractions were detected by Western blotting or dot blotting assays using anti-HA antibody (Boehringer-Mannheim).

***Xenopus* Oocytes and cRNA Preparation and Injection**

Xenopus oocytes were collected and incubated in 2 mg/ml collagenase (Type I, Sigma) in ND96 (Specialty Media) for 3–4 hr at room temperature. Oocytes were then washed four times with Barth's medium, transferred to L-15 medium, and allowed to recover at 18°C overnight before cRNA injection. Oocytes were maintained in L-15 at 18°C after cRNA injection, and experiments were performed between 1 and 7 days after injection. cDNAs encoding chicken nAChR subunits α4 and β2 in the PGH19 oocyte expression vector were linearized and used as templates for run-off transcription using the T7 promoter. Oocytes were injected with 20 nl of cRNA at a final concentration of ~0.05 ng/μl. α4 and β2 cRNAs were injected at a ratio of 1:1.

Electrophysiological Recording, Data Acquisition, and Analysis

Macroscopic currents were recorded with a GeneClamp 500 amplifier (Axon Instruments) using a two-electrode voltage clamp with active ground configuration. Electrode resistances ranged between 0.5 and 5 MΩ and were filled with 3 M KCl. Membrane potential was clamped to −70 mV; only oocytes with leak currents of <100 nA were used. The extracellular recording solution included (in mM): 82.5 NaCl, 2 KCl, 1 $CaCl_2$, 1 $MgCl_2$, and 10 HEPES (pH 7.5) (all reagents from Sigma). Uninjected and mock-injected oocytes did not respond to ACh, rendering the inclusion of atropine in the extracellular perfusion solution unnecessary. ACh (RBI) was prepared in extracellular solution at concentrations of 10 μM to 1 mM. Oocytes were perfused at ~5 ml/min and were exposed to sequential, 20 s applications of agonist with 5 min intertrial intervals. Stable baseline

responses to ACh (i.e., an intertrial variance of $<2.5\%$) are typically achieved within two to three trials under these recording conditions. Following an initial assessment of four sequential pretreatment responses to ACh, solutions containing either 1% column-passed PBS or column-purified lynx1 in PBS were applied to oocytes for 20 s. ACh-evoked macroscopic currents were recorded again, immediately after exposure to the test solution ($t = 0$) and at 5 min intervals thereafter ($t = 1$–5). Oocytes were perfused in control medium for 30 min before the next test solution was applied. Macroscopic currents were recorded and the rise times, amplitude, and time course of the elicited currents were analyzed using Pclamp6 (Axon Instruments). Graphical and statistical analyses utilized Origin 5.1 (Microcal Software).

Acknowledgments

We thank Dr. Marc Ballivet (University of Geneva) for cDNAs encoding chicken nAChR subunits α4 and β2. We would also like to thank Mary Beth Hatten, Carol A. Mason, Colin F. Fletcher, Monica Bravin, and Daniel Besser for critical reading of the manuscript; Richard Frederickson, Colin F. Fletcher, Dennis J. Sawchuk, and Susan Moriguchi for assistance with figures and/or cover design; Svetlana C. Maric, Wendy Lee, and Maduri Roy for technical assistance; and members of the Heintz lab for helpful discussions. This research was supported by the Howard Hughes Medical Institute, NIH NINDS P01 NS30532, AT Children's Project (I. I.-T.), The Rockefeller University, and NIH 5T32 GM07524 (J. M. M.).

Received March 8, 1999; revised March 26, 1999.

References

Adem, A., and Karlsson, E. (1997). Muscarinic receptor subtype selective toxins. Life Sci. *60*, 1069–1076.

Altschul, S.F., Gish, W., Miller, W., Myers, E.W., and Lipman, D.J. (1990). Basic alignment search tool. J. Mol. Biol. *215*, 403–410.

Basus, V.J., Song, G., and Hawrot, E. (1993). NMR solution structure of an α-bungarotoxin/nicotinic receptor peptide complex. Biochemistry *32*, 12290–12298.

Brakenhoff, R.H., Gerretsen, M., Knippels, E.M., van Dik, M., van Essen, H., Weghuis, D.O., Sinke, R.J., Snow, G.B., and van Dongen, G.A. (1995). The human E48 antigen, highly homologous to the murine Ly-6 antigen ThB, is a GPI-anchored molecule apparently involved in keratinocyte cell–cell adhesion. J. Cell Biol. *129*, 1677–1689.

Brakenhoff, R.H., van Dijk, M., Rood-Knippels, E.M., and Snow, G.B. (1997). A gain of novel tissue specificity in the human Ly-6 gene E48. J. Immunol. *159*, 4879–4886.

Brooks, B.R., Bruccoleri, R.E., Olafson, B.D., States, D.J., Swaminathan, S., and Karplus, M.K. (1983). CHARMM: a program for macromolecular energy minimization and dynamics calculations. J. Comput. Chem. *4*, 187–217.

Chang, L.S., Chou, Y.C., Lin, S.R., Wu, B.N., Lin, J., Hong, E., Sun, Y.J., and Hsiao, C.D. (1997a). A novel neurotoxin, cobratoxin b, from *Naja naja atra* (Taiwan cobra) venom: purification, characterization, and gene organization. J. Biochem. (Tokyo) *122*, 1252–1259.

Chang, L.S., Lin, J., Chou, Y., and Hong, E. (1997b). Genomic structure of cardiotoxin 4 and cobratoxin from *Naja naja atra* (Taiwan cobra). Biochem. Biophys. Res. Comm. *239*, 756–762.

Changeux, J.P., Bertrand, D., Corringer, P.J., Dehaene, S., Edelstein, S., Lena, C., Le Novere, N., Marubio, L., Picciotto, M., and Zoli, M. (1998). Brain nicotinic receptors: structure and regulation, role in learning and reinforcement. Brain Res. Rev. *26*, 198–216.

Chen, D., and Patrick, J.W. (1997). The α-bungarotoxin-binding nicotinic acetylcholine receptor from rat brain contains only the α7 subunit. J. Biol. Chem. *272*, 24024–24029.

Contant, C., Umbriaco, D., Garcia, S., Watkins, K.C., and Descarries, L. (1996). Ultrastructural characterization of the acetylcholine innervation in adult rat neostriatum. Neuroscience *71*, 937–947.

Coull, J.T. (1998). Neural correlates of attention and arousal: insights from electrophysiology, functional neuroimaging and psychopharmacology. Prog. Neurobiol. *55*, 343–361.

Cousin, X., Bon, S., Massoulie, J., and Bon, C. (1998). Identification of a novel type of alternatively spliced exon from the acetylcholinesterase gene of *Bungarus fasciatus*. Molecular forms of acetylcholinesterase in the snake liver and muscle. J. Biol. Chem. *273*, 9812–9830.

Davidson, F.F, and Dennis, E.A. (1990). Evolutionary relationships and implication for the regulation of phospholipase A2 from snake venom to human secreted forms. J. Mol. Evol. *31*, 228–238.

Descarries, L., Gisiger, V., and Steriade, M. (1997). Diffuse transmission by acetylcholine in the CNS. Prog. Neurobiol. *53*, 603–725.

Dominguez Del Toro, E., Juiz, J.M., Peng, X., Lindstrom, J., and Caido, M. (1994). Immunocytochemical localization of the α7 subunit of the nicotinic acetylcholine receptor in the rat central nervous system. J. Comp Neurol. *349*, 325–342.

Dufton, M.J., and Harvey, A.L. (1989). The long and the short of snake toxins. Trends Pharmacol. Sci. *10*, 258–259.

Everitt, B.J., and Robbins, T.W. (1997). Central cholinergic systems and cognition. Annu. Rev. Psychol. *48*, 649–684.

Fleming, T.J., OhUigin, C., and Malek, T.R. (1993). Characterization of two novel Ly-6 genes. Protein sequence and potential structural similarity to α-bungarotoxin and other neurotoxins. J. Immunol. *150*, 5379–5390.

Fletcher, C.H., Lachmann, P.J., and Neuhaus, D. (1994). Structure of a soluble form of the human complement regulatory protein CD59. Structure *2*, 185–199.

Fuse, N., Tsuchiya, T., Nonomura, Y., Menez, A., and Tamiya, T. (1990). Structure of the snake short-chain neurotoxin, erabutoxin c, precursor gene. Eur. J. Biochem. *193*, 629–633.

Gallagher, M., and Rapp, P.R. (1997). The use of animal modes to study the effects of aging on cognition. Annu. Rev. Psychol. *48*, 339–370.

Garside, S., and Mazurek, M.F. (1997). Role of glutamate receptor subtypes in the differential release of somatostatin, neuropeptide Y, and substance P in primary serum-free cultures of striatal neurons. Synapse *27*, 161–167.

Geula, C. (1998). Abnormalities of neural circuitry in Alzheimer's disease: hippocampus and cortical cholinergic innervation. Neurology *51*, S18–S29.

Gray, R., Rajan, A.S., Radcliffe, K.A., Yakehiro, M., and Dani, J.A. (1996). Hippocampal synaptic transmission enhanced by low concentrations of nicotine. Nature *383*, 713–716.

Gumley, T.P., McKenzie, I.F.C., and Sandrin, M.S. (1995a). Tissue expression, structure and function of the murine Ly-6 family of molecules. Immunol. Cell Biol. *73*, 277–296.

Gumley, T.P., McKenzie, I.F.C., and Sandrin, M.S. (1995b). Sequence and structure of the mouse ThB gene. Immunogenetics *42*, 221–224.

Hanninen, A., Jaakkola, I., Salmi, M., Simell, O., and Jalkanen, S. (1997). Ly-6C regulates endothelial adhesion and homing of CD8+ T cells by activating integrin-dependent adhesion pathways. Proc. Natl. Acad. Sci. USA *94*, 6898–6903.

Harvey, A.L. (1997). Recent studies on dendrotoxins and potassium ion channels. Gen. Pharmacol. *28*, 7–12.

Hung, C.C., Wu, S.H., and Chiou, S.H. (1998). Two novel α-neurotoxins isolated from Taiwan cobra: sequence characterization and phylogenetic comparison of homologous neurotoxins. J. Protein Chem. *17*, 107–114.

Im, W.B., Blakeman, D.P., Davis, J.P., and Ayer, D.E. (1990). Studies on the mechanism of interactions between anesthetic steroids and γ-aminobutyric acid A receptors. Mol. Pharmacol. *37*, 429–434.

Inoue, S., Oda, T., Koyama, J., Ikeda, K., and Hayashi, K. (1991). Amino acid sequences of nerve growth factors derived from cobra venoms. FEBS Lett. *279*, 38–40.

John, T.R., Smith, L.A., and Kaiser, I.I. (1994). Genomic sequences encoding the acidic and basic subunits of Mojave toxin: unusually high sequence identity of noncoding regions. Gene *139*, 229–234.

Jolkkonen, M., van Giersgergen, P.L., Hellman, U., Wernstedt, C., and Karlsson, E. (1994). A toxin from the green mamba *Dendroaspis*

angusticeps: amino acid sequence and selectivity for muscarinic m4 receptors. FEBS Lett. *352*, 91–94.

Kini, R.M., and Chan, Y.M. (1999). Accelerated evolution and molecular surface of venom phospholipase A2 enzyme. J. Mol. Evol. *48*, 125–132.

Kochva, E., Bdolah, A., and Wollberg, Z. (1993). Sarafotoxins and endothelins: evolution, structure, and function. Toxicon *31*, 541–568.

Kuhar, S.G., Feng, L., Vidan, S., Ross, M.E., Hatten, M.E., and Heintz, N. (1993). Changing patterns of gene expression define four stages of cerebellar granule neuron differentiation. Development *117*, 97–104.

Kumar, T.K., Jayaraman, G., Lee, C.S., Arunkumar, A.I., Sivaraman, T., Samuel, D., and Yu, C. (1997). Snake venom cardiotoxins—structure, dynamics, function and folding. J. Biomol. Struct. Dyn. *15*, 431–463.

Larramendi, L.M.H., and Viktor, T. (1967). Synapses on Purkinje cell spines in the mouse; an electron microscopic study. Brain Res. *5*, 15–30.

Le Goas, R., LaPlante, S.R., Mikou, A., Delsuc, M.A., Guittet, E., and Robin, M., Charpentier, I., and Lallemand, J.Y. (1992). α-Cobratoxin: a proton NMR assignments and solution structure. Biochemistry *31*, 4867–4875.

Maley, B.E., Newton, B.W., Howes, K.A., Herman, L.M., Oloff, C.M., Smith, K.C., and Elde, R.P. (1987). Immunohistochemical localization of substance P and enkephalin in the nucleus tractus solitarii of the rhesus monkey, *Macaca mulatta*. J. Comp. Neurol. *260*, 483–490.

Matthes, H.W., Smadja, C., Valverde, O., Vonesch, J.L., Foutz, A.S., Boudinot, E., Denavit-Saubie, M., Severini, C., Negri, L., Roques, B.P., et al. (1998). Activity of the δ-opioid receptor is partially reduced, whereas activity of the κ-receptor is maintained in mice lacking the μ-receptor. J. Neurosci. *18*, 7285–7295.

McGehee, D.S., Heath, M.J.S., Gelber, S., Devay, P., and Role, L.W. (1995). Nicotine enhancement of fast synaptic transmission in CNS by presynaptic receptors. Science *269*, 1692–1696.

Ohno, M., Menez, R., Ogawa, T., Danse, J.M., Shimohigashi, Y., Fromen, C., Ducancel, F., Zinn-Justin, S., Le Du, M.H., Boulain, J.C., Tamiya, T., and Menez, A. (1998). Molecular evolution of snake toxins: is functional diversity of snake toxins associated with a mechanism of accelerated evolution? Prog. Nucleic Acids Res. *59*, 307–364.

Picciotto, M.R., Zoli, M., Lena, C., Bessis, A., Lallemand, Y., LeNovere, N., Vincent, P., Pich, E.M., Brulet, P., and Changeux, J.P. (1995). Abnormal avoidance learning in mice lacking functional high-affinity nicotine receptors in the brain. Nature *374*, 65–67.

Robbins, T.W. (1997). Arousal systems and attentional processes. Biol. Psychol. *45*, 57–71.

Robbins, T.W., McAlonan, G., Muir, J.L., and Everitt, B.J. (1997). Cognitive enhancers in theory and practice: studies of the cholinergic hypothesis of cognitive deficits in Alzheimer's disease. Behav. Brain Res. *83*, 15–23.

Šali, A., and Blundell, T. (1993). Comparative protein modelling by satisfaction of spatial restraints. J. Mol. Biol. *234*, 779–815.

Sánchez, R., and Šali, A. (1997). Evaluation of comparative protein structure modeling by MODELLER-3. Proteins *1 (suppl.)*, 50–58.

Sánchez, R., and Šali, A. (1998). Large-scale protein structure modeling of the *Saccharomyces cerevisiae* genome. Proc. Natl. Acad. Sci. USA *95*, 13597–13602.

Sippl, M.J. (1993). Recognition of errors in three-dimensional structures of proteins. Proteins *17*, 355–362.

Strydom, D.J. (1979). The evolution of toxins found in snake venoms. In Handbook of Experimental Pharmacology, Volume 52, C.Y. Lee, ed. (New York: Springer-Verlag), pp. 258–275.

Udenfriend, S., and Kodukula, K. (1995). How glycosyl-phosphatidylinositol-anchored membrane proteins are made. Annu. Rev. Biochem. *64*, 563–591.

GenBank Accession Number

The GenBank accession number for the *lynx1* sequence reported in this paper is AF141377.